Available online at www.sciencedirect.com
SCIENCE DIRECT®
Sedimentary Geology 162 (2003) 5–24
Sedimentary Geology
www.elsevier.com/locate/sedgeo

Predicting the terrestrial flux of sediment to the global ocean: a planetary perspective

James P.M. Syvitski[a,*], Scott D. Peckham[a], Rachael Hilberman[a], Thierry Mulder[b]

[a] *Environmental Computation and Imaging Group, INSTAAR, University of Colorado, 1560 30th Street, Boulder, CO 80309-0450, USA*
[b] *Département de Géologie et d'Océanographie, UMR 5805 EPOC, Université Bordeaux I, Avenue des Facultés, 33405 Talence cedex, France*

Abstract

A new model for predicting the long-term flux of sediment from river basins to the coastal ocean is applied to a global data set of 340 river basins. The model is based on relief, basin area (or, averaged discharge), and basin-averaged temperature. Basin-averaged temperature is determined from basin location (latitude, longitude) and the lapse rate across the basin relief (hypsometric approximation). The sediment flux model incorporates climate through basin temperature and hydrologic runoff. Solutions are provided for each of the major hemispheric climate regions (polar, temperate and tropic). The model successfully predicts the pre-anthropogenic flux of sediment to within the uncertainties associated with the global observations (within a factor of two for 75% of rivers that range across five orders of magnitude in basin area and discharge). Most of the ''problem'' rivers are associated with low observational loads (often smaller rivers where anthropogenic impacts are often magnified, and temporal variability is high). Model predictions provide a baseline for researchers: (1) to question the quality of observational data where available and disagreement is greatest, (2) to examine a river basin for unusually large anthropogenic influences (i.e. causes of erosion or causes of hinterland sediment retention), and (3) to uncover secondary factors not addressed by our model (lithology, lakes). The model provides a powerful tool to address the impact of paleo-climate fluctuations (warmer/colder; wetter/drier) on the impact of sediment flux to the coastal ocean.

Keywords: Terrestrial flux; Global ocean; Climate fluctuations

1. Introduction

Marine sedimentary basins are the tape recorders of earth history, recording through proxy, climate variability, tectonic history and other large-scale dynamic events. Crucial to this understanding is knowledge of the ambient flux of sediment transported by rivers, as rivers contribute 95% of sediment entering the ocean (Table 1; Syvitski, in press). Knowing the average flux can help assess the impact of perturbations in the supply and transport of load. This paper provides a model for estimating this long-term flux of sediment to the ocean knowing a river's geographic location and a few basin characteristics. The paper explains how the model can be used to estimate the pre-anthropogenic flux of sediment and the role of climate change on sediment supply. The model is built on a large global database of environmental factors, river basin characteristics and sediment transport observations. We suggest that the physics of the problem is

* Corresponding author.
E-mail address: syvitski@colorado.edu (J.P.M. Syvitski).

0037-0738/$ - see front matter © 2003 Elsevier B.V. All rights reserved.
doi:10.1016/S0037-0738(03)00232-X

Table 1
Global estimates of the flux of sediment from land to the ocean (after Syvitski, 2003)

Transport mechanism	Global flux GT/year	Estimate grade	Reference
Rivers: suspended load	18	B^+	Milliman and Syvitski, 1992
bed load	2	B^-	Milliman and Syvitski, 1992
dissolved load	5	B^+	Summerfield and Hulton, 1994
Glaciers, sea ice, icebergs	2	C	Hay, 1994
Wind	0.7	C	Garrels and Mackenzie, 1971
Coastal erosion	0.4	D	Hay, 1994

contained within a database of global observations, with Earth having run the experiment in hundreds of locations under a wide range of environmental settings. We use a whole planet approach to assess the environmental factors, to allow for estimates in areas where there are no observational data.

Global databases on the very large rivers were first assembled to estimate the sediment flux to the world oceans (Holeman, 1980; Holland, 1981; Milliman and Meade, 1983). Milliman and Syvitski (1992) quadrupled the size of these databases (to 280 rivers) to emphasize the importance of the sediment flux from small mountainous rivers. This larger data set overcame the rather impossible task of otherwise extrapolating observations from large rivers to the smaller rivers. Milliman and Syvitski (1992) argued that the modern flux of fluvial sediment (20 GT/year) provides an over-estimate of pre-anthropogenic fluxes by 50%.

Whereas predicting the global ensemble flux of sediment to the ocean is one problem, developing a model to predict the flux from an individual river basin is another. A variety of factors influence the "natural" sediment load of a river, but the significant factors are the size of a drainage basin (Wilson, 1973; Milliman and Syvitski, 1992) and large-scale relief within the basin (Pinet and Souriau, 1988; Milliman and Syvitski, 1992; Harrison, 1994). Other influences largely scale with one of these two parameters. For example, local relief (Ahnert, 1970; Jansen and Painter, 1974) is correlated with large-scale relief (Summerfield and Hulton, 1994). Ice cover and ice-melt scales with solar radiation and relief (Andrews and Syvitski, 1994). Precipitation intensity is somewhat captured through basin relief (Fournier, 1960; Jansen and Painter, 1974; Hay et al., 1987), and runoff is correlated with basin area (Walling, 1987; Milliman and Syvitski, 1992; Mulder and Syvitski, 1996).

Mulder and Syvitski (1995) revised the global data set of Milliman and Syvitski (1992) by substituting maximum relief values for height classes. Mulder and Syvitski (1996) developed a deterministic relationship for predicting the load of rivers based on the large-scale relief and drainage area. Syvitski and Morehead (1999) developed the relationship in terms of a balance between a gravity-driven sediment yield (first term in 1) and potential energy (second term in 1):

$$\frac{\overline{Qs}}{\rho g^{1/2} A^{5/4}} = \beta \left(\frac{R}{A^{1/2}} \right)^n, \tag{1}$$

where $\overline{Qs}$ is the long-term sediment load (kg/s); R is relief defined as the highest point of elevation (m) minus the elevation (m) of the discharge station; A is basin area (km^2); ρ is grain density (2650 kg/m^3); g is acceleration due to gravity (9.8 m/s^2) and β and n are constants of proportionality. Solving Eq. (1) for $\overline{Qs}$ and using $n = 1.5$ (from regression analysis) yields:

$$\overline{Qs} = \alpha R^{3/2} A^{1/2}, \tag{2}$$

where $\alpha = \beta \rho g^{1/2} = 2 \times 10^{-5}$ [M L$^{-2.5}$ T^{-1}]. Syvitski and Morehead (1999) determined β to be dependent on climate and suggested $\alpha = 10^{-6}$ for cold northern rivers. Morehead et al. (in press) recently explicitly introduced basin temperature into Eq. (2) as:

$$\overline{Qs} = \alpha R^{3/2} A^{1/2} e^{k\overline{T}}, \tag{3}$$

where $\overline{T}$ is mean surface temperature of the drainage basin °C), and k and α are constants (2×10^{-5}, 0.1331, respectively). Syvitski (2002) applied Eq. (3) to 48 polar rivers and predicted the flux of sediment to within a factor of 2, across four orders of magnitude in basin area and discharge.

This paper tests the general applicability of Eq. (3) to an improved global river database, discusses the limitations of the database, provides important revisions to Eq. (3) using a planetary approach to basin climate, and provides examples of model application

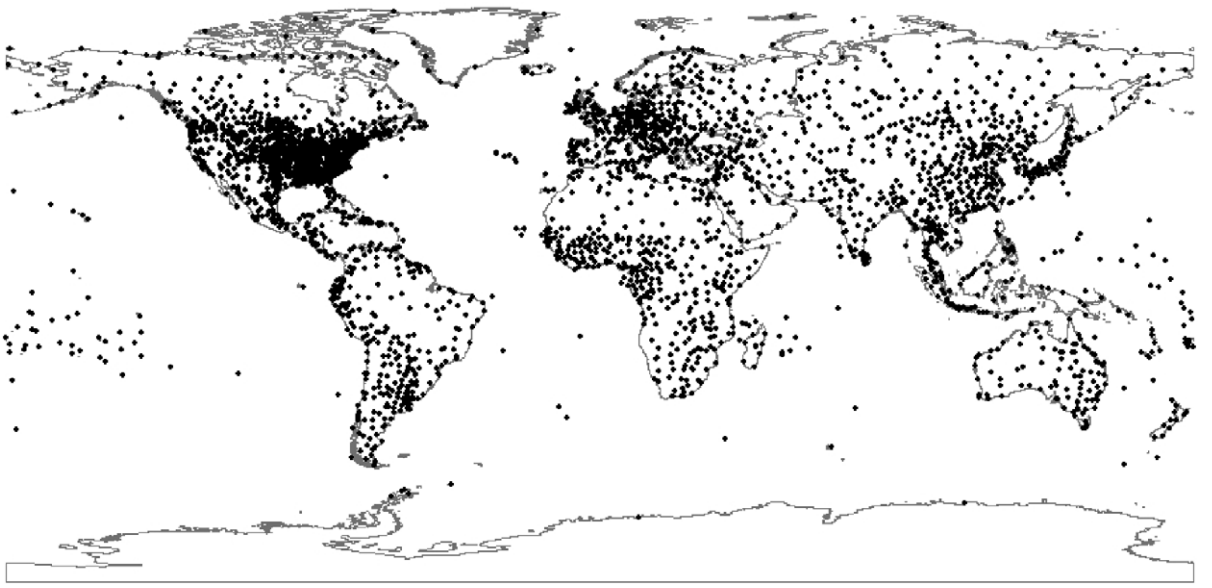

Fig. 1. Global distribution of 3423 met stations providing monthly averages on precipitation and temperature, with most stations reporting between 50 and 100 years of observations.

related to anthropogenic issues, global warming, and paleo-climate change scenarios.

2. Database

To analyze Eq. (3), a database of long-term averages of the temperature distributed throughout a river basin is required, as well as a method to predict basin temperature where direct observations are lacking. Analysis of Eq. (3) requires GIS information on river basin area and relief along with an estimate of the accuracy of these values. The exercise also requires a significant number of globally distributed rivers, each having useful (quantity and quality) observations on their sediment load and discharge of rivers, to allow for a planetary approach.

Load and discharge measurements came from the Milliman and Syvitski (1992, see references therein) database with corrections[1] and new data supplied by Milliman et al. (1995), Mulder and Syvitski (1995, 1996), Wang et al. (1998), Syvitski et al. (2000), Meybeck and Ragu (1996), and Syvitski (2002). The new river database consists of 340 rivers from a wide variety of sources.

Climate information is derived from an analysis of geographically located (latitude, longitude, altitude) meteorological data comprising 3423 global stations (NOAA NCDC: National Oceanic and Atmospheric Administration, National Climate Data Center). The database consists of monthly averaged precipitation and temperature observations, with most stations reporting observations of between 50 and 100 years duration (collected variably between the years 1700 AD and 1995 AD). Station locations largely reflect the global distribution of human population (Fig. 1). NCEP/NCAR (National Centers for Environmental Prediction/National Center for Atmospheric Research) ''Reanalysis'' data was provided by the NOAA-CIRES (Cooperative Institute for Research in Environmental Science) Climate Diagnostic Center, Boulder, Colorado (http://www.cdc.noaa.gov/). The reanalysis data was used to evaluate temperature at 17 pressure surfaces, and derive a 2.5° grid of global lapse rates (change in temperature with elevation). The lapse rates (Fig. 2) were calculated with pressure to height conversion formulas (Wallace and Hobbs, 1977). Surface temperature values (Fig. 3) were

[1] Corrections required due to data transfer errors and data quality errors.

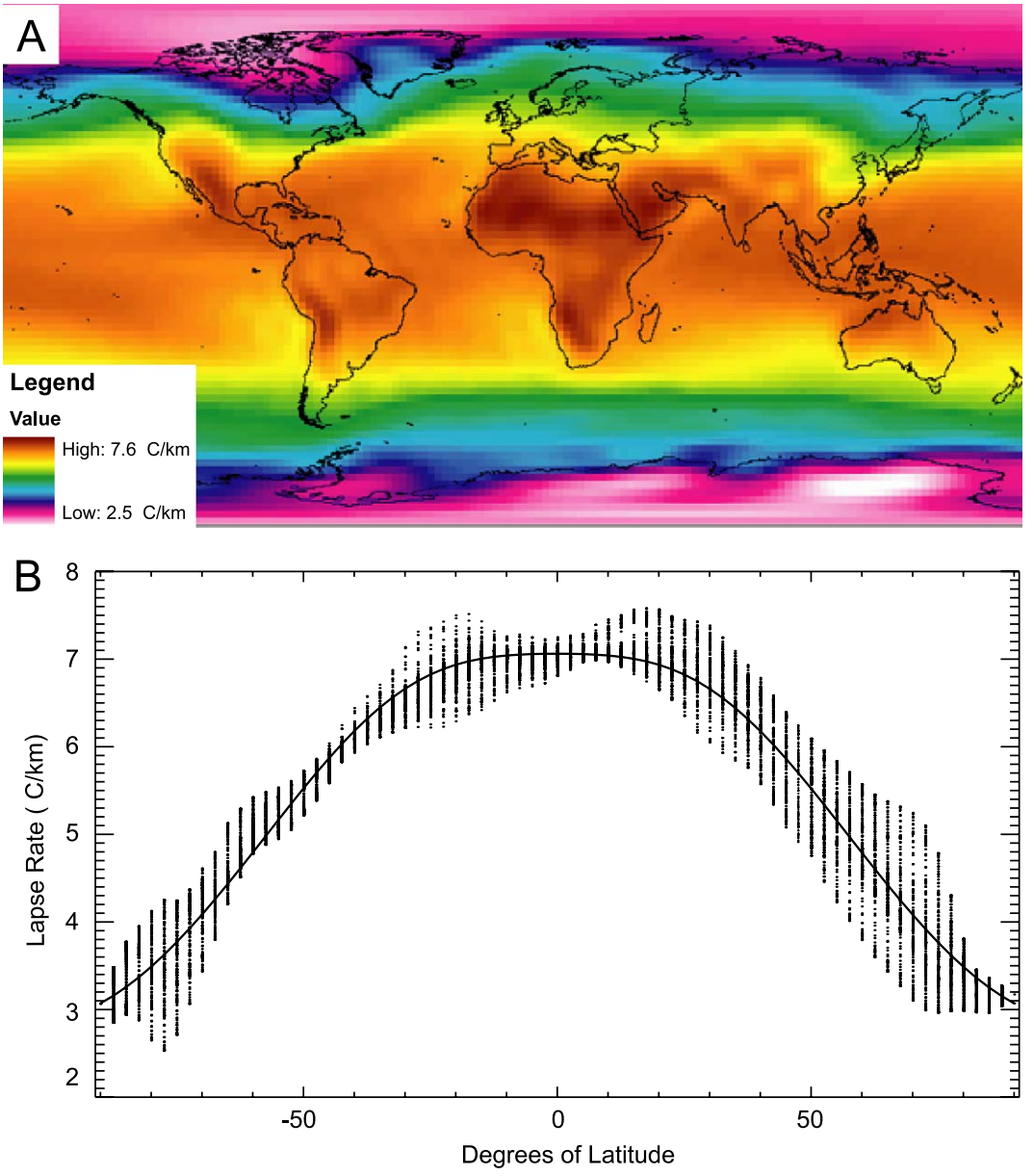

Fig. 2. (A) The NCEP/NCAR Reanalysis of global lapse rates [°C/km] on a 2.5° grid. Note the strong latitudinal banding. (B) Lapse rate [°C/km] and latitude for every pixel in a global grid (A) along with the predicted fit (Eqs. (5)–(7)).

calculated from the 1000-mb level NCEP-derived temperature, and then relating this 1000 mb grid to a surface pressure grid (Trenberth, 1992) to correct for elevation using the lapse rate.

The final database contains values on rivers draining into the ocean as measured at the most seaward gauging station.[2] River locations are from gauge station reports, published sources, or estimates from atlases. Large rivers (>25,000 km^2) were co-located

[2] These include stations that can be hundreds of kilometers from the coastline. For a full discussion, see Syvitski and Morehead (1999).

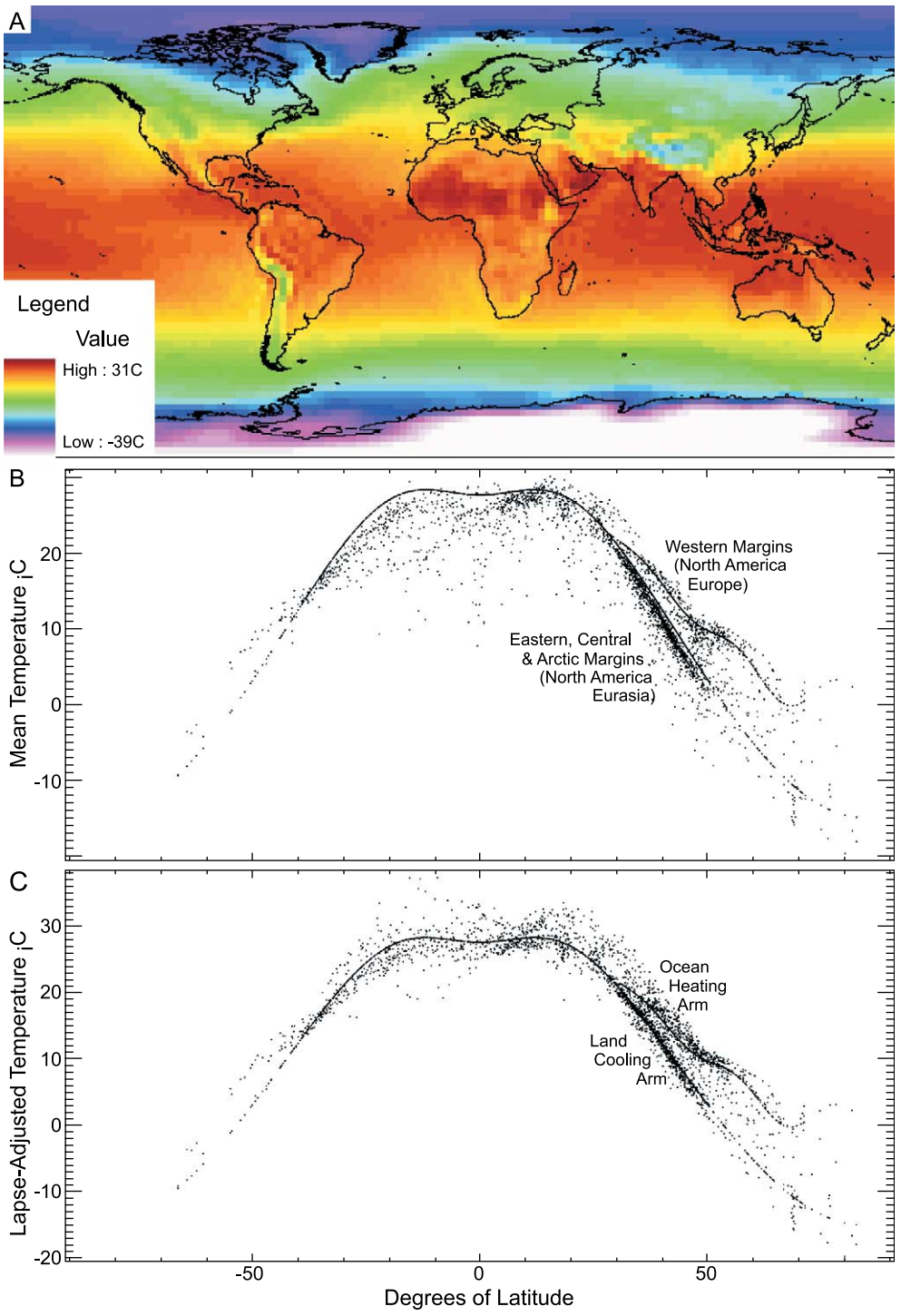

Fig. 3. (A) 2.5° grid of surface temperatures (see text). (B) Global station temperature versus latitude and the best-fit model (Eqs. (5)–(7)). (C) Lapse-adjusted temperature versus latitude shows the general tightening of the fit.

with the STN-30 (30 min simulated network typology) database of the University of New Hampshire-Global Hydrological Archive and Analysis System (UNH-GHAAS) that contains environmental information on >600 individual drainage basins in a GIS data compendium at 0.5° (lat., long.) spatial resolution (Vörösmarty et al., 2000a,b). The UNH data is based on ETOPO5 (Earth Topography-5 Minute) (Edwards, 1989) and incorporates corrections for hydrological stream flow errors. Maximum relief was determined from a 1 km global Digital Elevation Model (DEM) HYDRO1K elevation derivative database (http://edcwww.cr.usgs.gov/landdaac/gtopo30/hydro/index.html) and then verified on published maps.

3. Data quality

The data for our analysis is derived from a variety of sources, using a variety of methods, which warrants an overview of data quality. Reliability issues in the final database include differences between data sets, non-representative data, and lack of data or missing values. In short, uncertainty is introduced through missing data and combining different data sources. For example, the accuracy of the estimated latitudes and longitudes depends on the number and/or spread of the data points within a basin, and the STN-30 delineation of basin boundaries.

We compared the same variables where overlap occurred between the databases to estimate the level of agreement. When comparing drainage areas of the larger river basins, i.e. >25,000 km^2, the mean variance is ±1.3%. Some of the differences for defining basin area lay in the measurement techniques used by STN-30 compared to the often-unreported techniques used to define gauging station's upstream area. The STN-30 dataset is based on ETOPO5 and ARC/INFO flow direction algorithms. Errors may be introduced by artificial DEM topography, even though the STN-30 dataset incorporates corrections for most of these errors. When comparing location for basins (as used in the basin temperature calculation outlined below) with drainage areas <25,000 km^2, mean variance is ±1.0°, with the centroid of the drainage basin is estimated to be within ±200 km. This contributes one of the errors in arriving at a basin average temperature as measured at sea level (see discussion below).

Observational errors include loads estimated from too few samples; samples collected over too few years and therefore may not capture the high-energy events, measurement techniques, and human impacts. Meybeck et al. (in press) note that most "global river data" include load estimates that range from samples collected from simple surface bucket sampling, to depth-integrated sampling with multiple vertical profiles; discrepancies can exceed 100% on sediment concentration determined between sampling methods.

Observational uncertainties on the long-term sediment flux of rivers can therefore be large, and may range from a factor of two for estimates for well-monitored rivers (Meybeck et al., in press), to in excess of an-order-of-magnitude for poorly monitored rivers. Uncertainties in the later case are associated with short-term measurements of sediment load that may or may not contain the important transport events (see Morehead et al., in press). There can be order of magnitude year-to-year variation for many rivers. In 1977 the Eel River load was 0.6 kg/s, in 1965 the load was 4838 kg/s. Even large rivers with reduced inter-annual variability, like the Mississippi, have order of magnitude ranges (1963: 2916 kg/s vs. 1951: 16,524 kg/s). Inman and Jenkins (1999) note the El Nino/Southern Oscillation-induced climate changes recur on a multidecadal time scale that is in general agreement with the Pacific/North American climate pattern: a dry climate extending from 1944 to about 1968 and a wet climate extending from about 1969 to the present. Sediment loads measured in any one of these periods provide very different mean load estimates, with the wet period contributing sediment flux about five times greater than the dry period. Similarly, in East Africa a sharp rise in precipitation following a decade of relatively low rainfall is concomitant with sharp increases in sediment yields (Wasson, 1996).

It is difficult to assess the impact of changes in the flux of sediment to the oceans because of the conflicting impacts of man (Syvitski, in press). Globally, soil erosion is accelerating (e.g. deforestation, agriculture practices), while at the same time sediment flux to the coastal zone is globally decelerating (e.g. water diversion schemes, dams). There are over 36,000 large reservoirs in the world. Between 1951

and 1982 large dams were being constructed at a rate of 900 per year (Vörösmarty et al., 2003). Unfortunately this period is when most of the world river loads were obtained. Where known we used the pre-dam river loads in our database (e.g. Colorado, Mississippi, Krishna, Nile, Han, Yesil-Irmak, Sakarya, Kizil-Irmak, Ebro, Columbia, Rio Grande, Orange, Zambesi, Savannah, Volta, Roanoke, Altamaha). However, there remain many rivers in the database whose fluxes strongly reflect the impact of reservoir impoundment of sediment.

Other sources of error are caused by a mismatch between years of observations in reported water discharge (often much longer) and reported sediment discharge (see Syvitski et al., 2000), and by combining data from different countries that use different measurement techniques (see Bobrovitskaya et al., 1997). We were unable to verify water discharge for 73 out of the 340 rivers in the data set and there are missing values of either relief or drainage area on 20 rivers.

4. Computing average values for river basins

Eq. (3) for *Qs* requires a single mean temperature representative of the basin as a whole. The area-average of a property (i.e. temperature, elevation, or latitude) that varies spatially throughout a river basin is computed as an area-weighted average of the gridded value for all pixels in the basin. Let N_k be the number of pixels that contribute flow to the kth pixel in the gridded DEM, and let A_k be the total area spanned by this set of pixels; the contributing area for the kth pixel. Let P_j denote the property value that is stored for the jth pixel, and let da_j denote the area spanned by the jth pixel. The area-weighted basin average is computed as:

$$V_k = \frac{1}{A_k}\sum_{j=1}^{N_k} P_j da_j. \tag{4}$$

At the Earth's equator (latitude zero), 1° spans about 111.12 kilometers. At other latitudes, the east–west dimension is reduced by the factor cos (lat.). This means that for "geographic" DEMs, da_j varies with latitude and will impact the calculation of A_k. If a quantity like temperature is parameterized in terms of latitude, longitude and altitude (see below), then a basin-averaged location and altitude is first computed and used in the formula to obtain a basin-averaged temperature value.

5. Parameterization of temperature

Meteorological stations in the climate database used in this study are not distributed in sufficient spacing to be useful in quantifying the temperature within a drainage basin. Polar, desert and mountainous regions have poor distribution of climate data (Fig. 1). To compensate we have developed a simple method to approximate the temperature (within 3 °C) at any location on earth. Fig. 2B shows a plot of lapse rate [°C/km] with latitude for every pixel in a global grid of lapse rates (Fig. 2A). Each pixel in the grid spans 2.5° latitude by 2.5° longitude. Due to the overall parabolic shape of the curve with a dip near the top, the following nonlinear fitting functions were used to approximate the data.

$$L(x) = (a_0x^2 + a_1)\{1 - a_2\exp[-(x/a_3)^2]\}$$
(modified quadratic) (5)

$$L(x) = [a_0\cos(a_1x)]\{1 - a_2\exp[-(x/a_3)^2]\}$$
(modified cosine) (6)

$$L(x) = [a_0\cos(a_1x) + a_2]\{1 - a_3\exp[-(x/a_4)^2]\}$$
(modified cosine 2) (7)

The bracketed factor with the exponential was used to model the dip in the curve near the equator, which is known to be due to the effect of clouds (reflectance, evaporative cooling). Here L is lapse rate [°C/km], x is latitude [°], and the subscripted parameters are found by nonlinear regression.

Given the best-fit parameters (Table 2), Eqs. (5)–(7) are used to remove the effect of elevation on temperature from the meteorological data of 3423 mean annual temperatures. That is, the quantity

$$T_0 = T + [L(x)H] \tag{8}$$

is computed for each station, where H is the elevation [km], x is the latitude [°], L is the estimated lapse

Table 2
Regression coefficients on lapse rate and temperature models

Adjusted temperature versus latitude:
Modified Cosine2 (Eq. (7)): $a_0 = 25.25$; $a_1 = 0.03719$; $a_2 = 10.36$; $a_3 = 0.2220$; $a_4 = 18.13$
Quadratic (Eq. (5)): $a_0 = -0.01010$; $a_1 = 29.67$; $a_2 = 0.06516$; $a_3 = 8.087$
Lapse rate versus latitude:
Modified Cosine2 (Eq. (7)): $a_0 = 2.609$; $a_1 = 0.030$; $a_2 = 5.464$; $a_3 = 0.1252$; $a_4 = 33.77$
Quadratic (Eq. (5)): $a_0 = -0.0001121$; $a_1 = 2.363$; $a_2 = -2.052$; $a_3 = -104.9$

rate [°C/km] and T [°C] is the mean annual temperature for the station. Fig. 3A shows the planetary grid of mean temperatures, and the temperature distribution with latitude (Fig. 3B), and when the temperature at a location is corrected for its elevation (Fig. 3C). For latitudes north of about 28°N, the data splits into two arms. This effect is almost wholly accounted for by noting whether the predominant winds at the station were coming from the sea (warmer) or from land (colder). Stations that plot on the upper arm are at latitudes from 28°N and 58°N and longitude from −180° and −100° (i.e. west coast of North America), or longitude from −40° and 30° (i.e. western Europe). The remaining stations plot on the lower arm, including those that lie along the eastern and northern coasts of North America and Eurasia. Separate fitting curves were used for each of the two arms.

The mean annual temperature for each station was predicted from latitude, longitude and altitude via the formula:

$$T(x, \theta, H) = T_0(x, \theta) - [L(x)H]. \quad (9)$$

Fig. 4 plots the observed versus predicted temperatures for each station. Predicted temperatures are

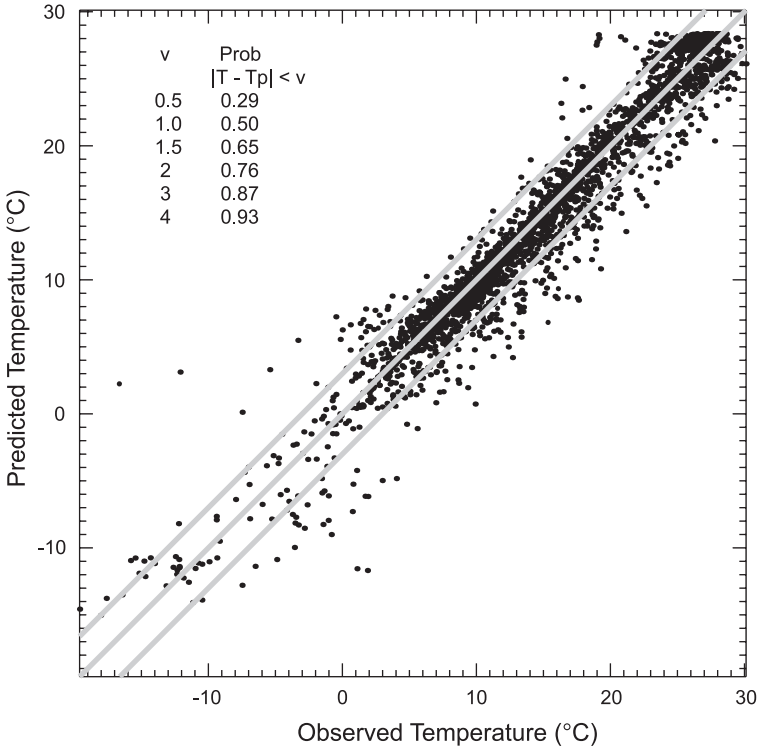

Fig. 4. Observed versus predicted temperatures for each station. Inset table shows the percentage of data points, out of 3423 stations, for which the absolute value of the difference between the reported temperature and the predicted temperature is less than a given number, v. Half of the data falls within 1 °C of our prediction, and 82% falls within 2.5°.

typically within 3 °C of observed temperatures (see uncertainty discussion below).

6. Improved sediment flux models

To apply Eq. (3) to our river basin data, we divided the entries into the basic climate zones (polar: $\overline{T} < 0$ °C, temperate: $\overline{T} > 0$ °C and latitude >30°, tropics: latitude <30°) with the hemispheres kept separate. The polar region defines river basins with some of the following characteristics (Syvitski and Andrews, 1994; Syvitski, 2002): significant proportion of precipitation falls as snow, snowmelt and or glacial-ice melt dominated discharge, short discharge season in late spring through summer, frozen active (soil groundwater) layer for much of the year, discontinuous to continuous permafrost in some or all of the drainage basin, minor contribution from convective rainfall, precipitation largely from frontal systems, and moderately low freeze–thaw events within the sediment-producing alpine weathering environments.

The temperate region provides the transition region between polar and tropical regions, resulting in rainfall discharge often of greater importance than snowmelt discharge, a larger groundwater contribution to discharge, precipitation from both frontal and convective systems, intense convective rainfall events, and a high number of freeze–thaw events in the alpine weathering zone. The tropics, including the equatorial regions, are dominated by: high year-round temperatures, intense convective rainfall, strong monsoon periods outside of the desert regions of Africa, and strong chemical weathering with landslides common.

The average basin temperature in our database falls nicely into the discrete climate zones of −10, 10 and 25 °C, respectively, for polar, temperate and tropical regions (Table 3). Within these zones there is a wide variance in basin area and relief for all zones except the temperate rivers of the southern hemisphere, which are dominated by relatively small area (and thus discharge) New Zealand and southern Australian rivers. The zones demonstrating the highest sediment production or yield (load divided basin area) were the tropics of the northern hemisphere followed by the southern temperate zone (Table 3). The polar rivers show the lowest values in sediment yield.

Eq. (3) can be rewritten as:

$$Q_s = \alpha_3 A^{\alpha_4} R^{\alpha_5} e^{kT} \tag{10}$$

to allow the coefficients to be determined by multiple-regression analysis based on groupings of river basins within each climate zone (Table 4). Lumping the

Table 4
Regression coefficients on $Q_s = \alpha_3 A^{\alpha_4} R^{\alpha_5} e^{kT}$

Global sector	No. of rivers	α_3	α_4	α_5	k	R^2
Polar ($T<0$ °C)*	48	2×10^{-5}	0.50	1.50	0.1	0.76
Temperate N (lat.>30°N, $T>0$ °C)	162	6.1×10^{-5}	0.55	1.12	0.07	0.63
Tropics N (lat. 0–30°N)	62	0.31	0.40	0.66	−0.1	0.58
Tropics S (lat. 0–30°S)	42	0.57	0.50	0.37	−0.1	0.67
Temperate S (lat.>30°S, $T>0$ °C)	26	1.3×10^{-3}	0.43	0.96	0	0.54

T is basin-average temperature (°C), A is drainage basin area (km^2), R is the maximum relief from sea level to the mountain-top (m), Qs is long term sediment load (kg/s).

Table 3
Averaged drainage basin characteristics by sector

Global sector	T	L	A	R	Qs	Y	Q
Polar ($T<0$ °C)*	−9.5	1232	390,000	1977	219	120	2666
Temperate N (lat.>30°N, $T>0$ °C)	9.9	667	114,000	1724	581	549	981
Tropics N (lat. 0–30°N)	20.3	1050	251,000	2552	1602	3648	3799
Tropics S (lat. 0–30°S)	22.7	1451	458,347	1875	1299	823	6570
Temperate S (lat.>30°S, $T>0$ °C)	9.2	434	68,000	1698	168	2999	502

T is basin-average temperature (°C), L is length (km) of rivers, A is drainage basin area (km^2), R is relief from sea level to the mountain-top (m), Qs is sediment load (kg/s) of rivers, Y is sediment yield (T/km^2/yr), i.e. Qs/A, Q is discharge (m^3/s).

world's river basins into climate zones helps to even out the otherwise dominance of 162 basins from the temperate region of the northern hemisphere, but also highlights the bare minimum of 26 basins to represent the Southern temperate zone. The delineation of climate into zones and its impact on sediment load is obvious with the cold regions sensitive to relief (large α_5) compared to their tropical counterparts (small α_5) (Table 4). The colder the basin temperature, the lower the predicted loads (i.e. k being positive); the warmer the temperature, the higher the loads (i.e. k is negative) (Table 4).

To compare the impact of climate on sediment loads we developed four scenarios where we could, in effect, move a basin similar in basin area and relief to the various climate zones (Fig. 5). We assumed an ideal temperature for each of the climate zones: −10 °C for polar, +10 °C for temperate, and +25 °C for the tropical basins. All of the climate zone predictions were generally similar, with the large area and high relief basin being predicted to produce the highest sediment loads, and similarly the low relief and small area basin producing the smallest sediment loads. At the detail level, the differences were large (Fig. 5). The higher sediment yields from tropical rivers produce the most sediment when relief is held low (scenarios 1 and 4: Fig. 5). While all climate zones produced high volumes of sediment when the relief and basin areas were large, the temperate rivers were found to be the rivers with the highest sediment yield. Is this an impact of humans (the greatest population is located in this zone), or does this show the great impact of high numbers of freeze–thaw events in the alpine environments of the temperate zone?

There is a direct relationship between drainage basin area and the volume of water discharged to

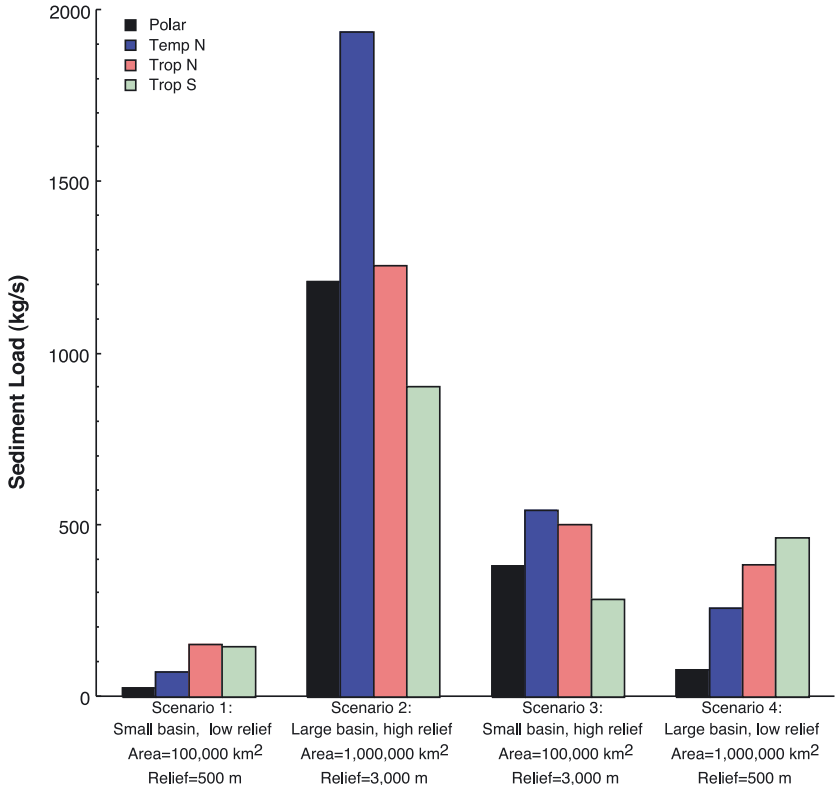

Fig. 5. Sediment load prediction scenarios based on $Qs = \alpha_3 A^{\alpha_4} R^{\alpha_5} e^{kT}$ and coefficients listed in Table 4. An ideal temperature for each of the climate zones was provided as −10 °C for polar, +10 °C for temperate, and +25 °C for the tropical basins.

the sea. Hydrological runoff, Θ, is dependent on three factors: (1) the amount of precipitation (P) that falls on the drainage basin, (2) the amount of water lost to evaporation (E) including evapotranspiration, and changes in the long term storage (S) of water including changes in permanent snow fields, glaciers, lakes and deep groundwater reservoirs. Thus,

$$\Theta = P - E \pm S, \tag{11}$$

with discharge, Q, being defined as:

$$Q = \Theta / A. \tag{12}$$

Since the distribution of drainage areas in our basins range over five orders-of-magnitude (90–7,500,000 km^2) and the vast majority of these basins have only one order-of-magnitude range in runoff values (50–500 mm/year), then there is a relatively good chance of a relationship being found between discharge and area (Table 5) such that:

$$Q = \alpha_1 A^{\alpha_2}. \tag{13}$$

Table 5 is based on fewer rivers than Table 4, and there are too few rivers in the southern temperate zone to solve for the regression coefficients. Still in the other zones, there is a very good relationship found between discharge and basin area. If the same rivers were used to develop Table 4 and Table 5, then it would be possible to substitute Q for A in Eq. (10). To accommodate the missing values, multiple-regression analysis was then done on the Table 5 rivers to solve for sediment load as a function of discharge, relief and temperature (Table 6):

$$Qs = \alpha_6 Q^{\alpha_7} R^{\alpha_8} e^{kT}. \tag{14}$$

Based on this solution, it is possible to redo the sediment load scenarios allowing for discharge volume and relief to define the end member conditions (Fig. 6). We again assumed an ideal temperature for each of the climate zones: −10 °C for polar, +10 °C for temperate, and +25 °C for the tropical basins. While there are similarities between Figs. 5 and 6, as would be expected with (Table 5) and a substitution of Eq. (13) into Eq. (10), there are differences at the detail level. For example, the basins in the southern tropics differ from basins in the northern hemisphere tropics in terms of sediment production, when discharge levels are held high and relief is varied (scenarios 2 and 3: Fig. 6). Polar rivers show the greatest sensitivity to relief for small discharge rivers (scenarios 1 and 3: Fig. 6).

Table 5
Regression coefficients on $Q = \alpha_1 A^{\alpha_2}$

Global sector	No. of rivers	α_1	α_2	R^2
Polar ($T<0$ °C)*	34	0.093	0.82	0.89
Temperate N (lat.>30°N, $T>0$ °C)	128	0.039	0.85	0.75
Tropics N (lat. 0–30°N)	53	0.53	0.70	0.76
Tropics S (lat. 0–30°S)	36	0.11	0.74	0.66
Temperate S (lat.>30°S, $T>0$ °C)	16 – not sufficient data	?	?	?

T is basin-average temperature (°C), A the drainage basin area (km^2), Q is average discharge (m^3/s).

Table 6
Regression coefficients on $Qs = \alpha_6 Q^{\alpha_7} R^{\alpha_8} e^{kT}$

Global sector	No. of rivers	α_6	α_7	α_8	k	R^2
Polar ($T<0$ °C)*	34	1.3×10^{-4}	0.55	1.5	0.1	0.78
Temperate N (lat.>30°N, $T>0$ °C)	128	1.1×10^{-3}	0.53	1.1	0.06	0.49
Tropics N (lat. 0–30°N)	53	2.0	0.45	0.57	−0.09	0.54
Tropics S (lat. 0–30°S)	36	162	0.65	−0.05	−0.16	0.76
Temperate S (lat.>30°S, $T>0$ °C)	16	?	?	?	?	?

T is basin-average temperature (°C), H is maximum relief from sea level to the mountain top (m), Qs is long term sediment load (kg/s), Q is average discharge (m^3/s).

7. Temperature versus precipitation as a controlling factor

While the impact of basin size and relief as controlling factors on a river's sediment load is generally accepted (Milliman and Syvitski, 1992), this paper contributes to the growing evidence that temperature plays an important (albeit secondary) role.

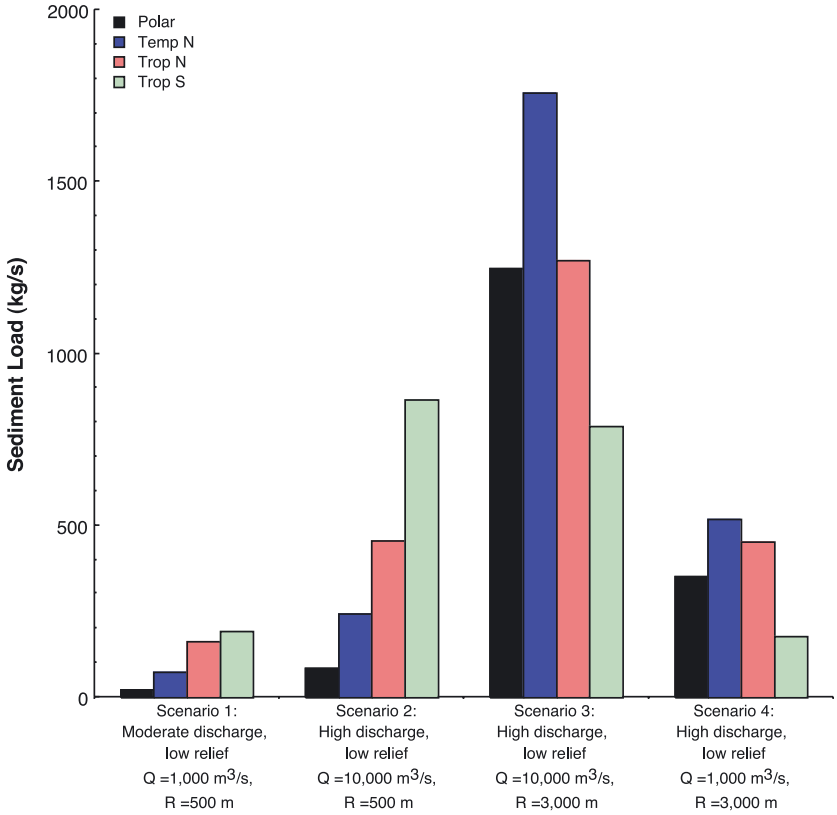

Fig. 6. Sediment load prediction scenarios based on $Q_s = \alpha_6 Q^{\alpha_7} R^{\alpha_8} e^{kT}$ and coefficients listed in Table 6. An ideal temperature for each of the climate zones was provided as −10 °C for polar, +10 °C for temperate, and +25 °C for the tropical basins.

McCave (1984) provides an early review of the temperature-dependence aspect of erosion rate, and the nature of the exponential form of the term in (Eq. (10) or Eq. (14)). The average temperature has been long known to influence the rate of chemical breakdown of the rocks (Berner, 1978), and includes an exponential impact of temperature on this rate. More recent papers have explicitly defined the role of temperature on river loads (Harrison, 2000).

However we argue that basin-averaged temperature has influence in excess of its impact on soil formation or soil erosion. Temperature also defines the polar feedbacks (frozen soils, snow and ice melt dominated discharge, frozen river beds, lack of convective rainfall) and the temperate zone feedbacks (snow melt, increasing lapse rate, freeze–thaw cycles, increasing convective rainfall). Temperature also defines the tropical zone feedbacks (convective rainfall–monsoons and typhoons, soil formation, tropical canopy). Temperature also controls the pathway of precipitation, from storage as ice and snow in the polar and alpine regions, to rates of evaporation including groundwater as well as other precipitation-to-discharge dynamics. Delayed precipitation, from snow or ice-melt is the main control on the discharge dynamics of many temperate rivers, even for large rivers like the Mississippi.

Most interesting was the lack of success in precipitation (rather than through discharge as given in Eq. (14)) in being identified as strong (albeit secondary) controlling influence on a river's sediment load. In fact the study originally set out to demonstrate this influence. We applied most of the known precipitation indices (mean, monthly maximum, Fournier index, aridity index) without success in improving the model's predictability.

8. Uncertainty analysis

The "fractional uncertainty" formula associated with Eq. (10) is (Taylor, 1982, p. 73):

$$\frac{\delta Qs}{Qs} = \sqrt{\left(\alpha_4 \frac{\delta A}{A}\right)^2 + \left(\alpha_5 \frac{\delta R}{R}\right)^2 + (k\delta T)^2}. \quad (15)$$

Note that Eq. (15) is dimensionless, and k has units of [1/°C]. With $\delta A/A$ estimated at 1.3% and $\delta R/R$ estimated at 1%. $\delta T = 3.0$ (with 87% confidence) when compared to individual climate stations (Fig. 3A). δT ranges from 3.0 for small basins and < 1.0 for larger basins, with a global average of 2.0.

$$\delta Qs = 0.2Qs, \text{ and} \quad (16)$$

$$Qs' = Qs \pm \delta Qs = Qs(1 \pm 0.2). \quad (17)$$

Uncertainty in T turns out to be the dominant contribution to the uncertainty in Qs. Based solely on errors in inputs, there is a high probability that the observed load, Qs' will fall between 0.8 Qs and 1.2 Qs, where Qs is our prediction or "best guess".

The uncertainty analysis of the sediment load model (10) shows that most of the rivers are relatively well predicted (Fig. 7). Seventy-five percent of our rivers have their sediment loads predicted *within* a factor of 2 (see Fig. 8) of the observed, and thus error in inputs to our formula for Qs is not solely responsible for the discrepancy. Rather, error in the model for Qs, and/or the observed values Qs' are greater than error due to uncertainty in input variables.

Based on a geometric argument, the fractional uncertainty for DEM-derived contributing basin area can be estimated as:

$$\frac{\delta A}{A} \approx 3.5\sqrt{\frac{\Delta A}{A}}, \quad (18)$$

where δA is uncertainty, A is actual basin area, and ΔA is the area of a pixel, which is about 1 km^2 (at the

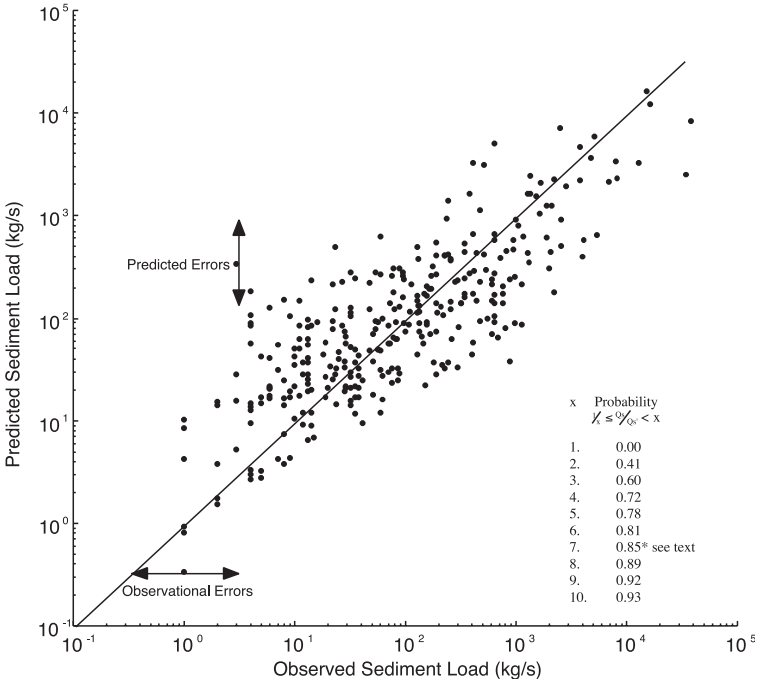

Fig. 7. Sediment load prediction based on predicted basin temperature, reported drainage area, DEM relief using $Qs = \alpha_3 A^{\alpha_4} R^{\alpha_5} e^{kT}$ and coefficients listed in Table 4. Observational errors include loads estimated from too few samples; samples collected over too few years, monitoring that does not capture the high-energy events, measurement techniques, and human impacts. Predicted errors include those related to input variables, and impact of local geography (e.g. lakes) or local geology (highly erodible rocks).

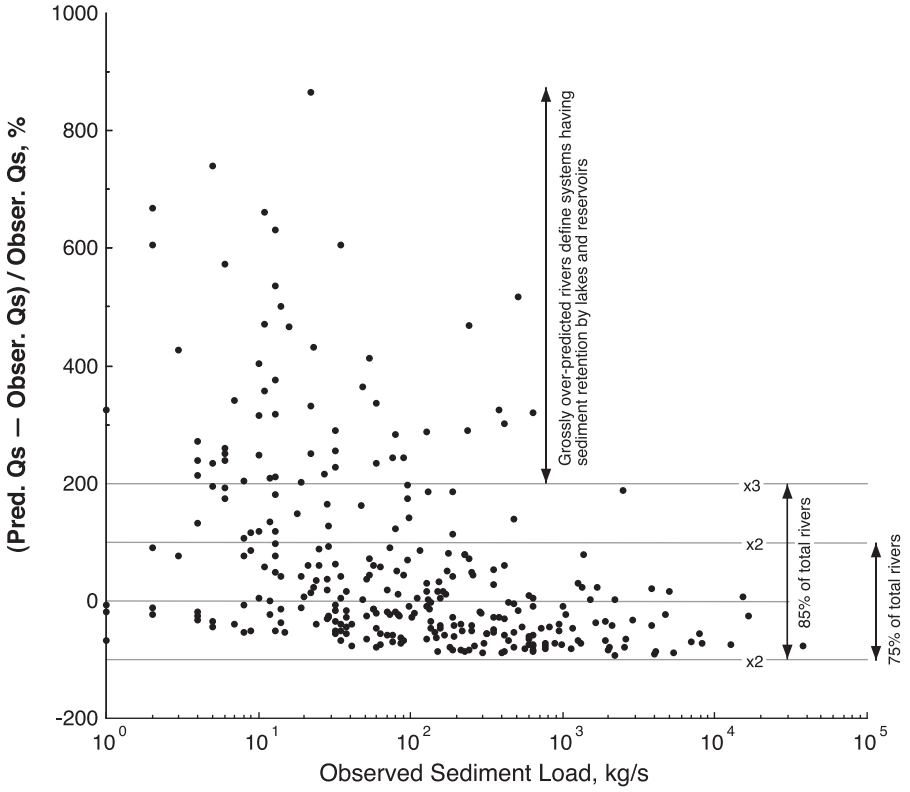

Fig. 8. Differences between predicted sediment loads ($Qs = \alpha_3 A^{\alpha_4} R^{\alpha_5} e^{kT}$) and observations of 320 rivers. Differences relate equally to uncertainties in observations as well as uncertainties in model predictions. Lakes and reservoirs are associated with sediment retention and identify many of the rivers with over-predicted loads (negative values). Most of the under-predicted rivers are associated with smaller rivers where anthropogenic impacts are magnified.

equator) for GTOPO30 and HYDRO1K and $\approx$ 3087 km^2 for the 1/2° STN-30 DEM. The formula shows how fractional uncertainty of basin area depends on pixel size, ΔA, when areas are estimated using DEMs.

9. Application of the sediment load model to anthropogenic issues

Uncertainties regarding the long-term load of rivers are of equal magnitude in both observations and predictions (Figs. 7 and 8). Thus for rivers where agreement is not good, it is not always possible to assign "fault" with either the model or the observations. Observational uncertainties include: (1) estimates from too few samples (e.g. Abitibi, Babbage, Attawapiskat) where monitoring does not capture the high-energy events, (2) measurement techniques, and (3) human impacts. Prediction uncertainties include those related to input variables (discussed above), and those related to either local geography (e.g. lakes), or local geology (e.g. highly erodible rocks).

Those rivers whose loads are grossly over-predicted or grossly under-predicted provide insight into where the "fault" may lie, if examined for cause. A number of rivers were found to have incorrect input data (human error). The area of the Senegal River upstream of the gauging station was found to be 3.1 times too large. The Mitchell River in the observational data had sediment loads for a river in NE Australia but input parameters defined a Mitchell River located in SE Australia. The Volga River had a maximum relief 7.2 times too small. When corrected, all three rivers were well predicted.

Lakes and reservoirs are known filters of sediment load and account for the rivers in our database with

grossly over-predicted loads. Vörösmarty et al. (2003) estimates that 30% of the global sediment flux is trapped behind large reservoirs. The Tagus (Tejo) River in Portugal was subsequently identified as one of the world's most reservoir-impacted rivers. Other examples include: the Odra (Oder) that drains the Lake District of Poland; the highly engineered Rhine (Germany) with its alpine load is filtered by Lake Constance; the Omoloy (Russia) that drains hundreds of thermokarst lakes; the Elbe (Germany) that is filtered by large reservoirs surrounding Brandenburg, Potsdam and Berlin, the lake-filtered Derwert (Tasmania) and Neveri (Venezuela); and Rangitaiki (NZ) filtered through the Aniwhena hydro-station.

To correct for the Trapping Efficiency, *TE*, of lakes and reservoirs the Brune equation can be used for lakes and reservoirs >0.5 km^3 (Brune, 1953; Ward, 1980; Vörösmarty et al., 1997, 2003):

$$TE = 1 - (0.05/\Delta\tau_r^{1/2}) \tag{19}$$

$$\Delta\tau_r = \frac{v}{Q} \tag{20}$$

where $\Delta\tau_r$ = water residence time change, v = volume of reservoir (km^3), and Q = discharge at basin mouth of the reservoir (km^3/year). To correct *TE* for small lakes and reservoirs (<0.5 km^3), the Brown equation (Verstraeten and Poesen, 2000) can be applied:

$$TE = 100\left(1 - \frac{1}{1 + 0.0021D\dfrac{C}{W}}\right) \tag{21}$$

where D depends on reservoir geometry (ranges 0.046–1, with a mean value of 0.1), and C = reservoir storage capacity (m^3), and W = drainage area above the reservoir. When applied to the grossly over-predicted rivers with lakes or reservoirs (see Fig. 8), Eqs. (19) and (21) correctly adjust the predicted sediment load to fall within a factor of two of observed loads.

The grossly under-predicted rivers are largely located in areas of elevated soil erosion due to human impact. The Huang (Yellow) River (PRC) is known for its elevated sediment discharge due to farming perturbations across its loess hills (Milliman et al., 1987; Wang et al., 1998). The Tseng Wen and the Erhain rivers (Taiwan) show the impact on erosion of road construction, and the subsequent farming on very steep slopes. The Waipaoa River (NZ) sees the combined impact of landslides and land use. Three heavily populated and impacted rivers in India (Godavari, Narmanda, Manuk) have grossly elevated sediment yields. Large river basins mitigate the impact of local perturbations. An excellent example of the impact of humans on a small watershed is the Lanyang River basin, Taiwan, where two large road construction projects increased sediment load export to the coast by more than tenfold, for a period of 2–4 years following each disturbance (Kao and Liu, 2001, 2002).

Human impact on the flux of sediment to the global ocean is well recognized (Berner and Berner, 1987; Hu et al., 2001). Land use is the dominant control on particulate fluxes in areas of low relief and large-scale urbanization, in contrast to mountainous regions where natural processes may still dominate (Wasson, 1996). Land clearing in low relief areas increases sediment yields by more than an order of magnitude (Douglas, 1967). One exception in our database, to the anthropogenic cause of elevated loads, is the turbid Copper River (Alaska) that drains one of the world's largest ice fields outside of Greenland and Antarctica.

The proposed sediment load model (10), therefore provides a convenient method to determine the level of human impact on reported sediment load observations. It also provides a method to determine the reliability of input parameters used in the predictions.

10. Application of the load model to global warming

Over the next hundred-year period, sea level fluctuations will not greatly impact the drainage areas of rivers, and denudation rates are too slow to impact the relief of these basins. The climate parameters of Eqs. (10) and (14), that of temperature and precipitation (i.e. via discharge), provide insight into the consequences of climate scenarios. Basin-averaged temperatures will fluctuate between years, but it is only across decades that a warming or cooling event will affect the flux of sediment off a drainage basin.

In the Arctic, the likely location of short-term climate warming, there could be large-scale release of stored water, as melt of permanent snow-fields, ablation of glaciers, or melt of permafrost occurs

(Syvitski et al., 1998). When applied to the high-latitude Colville River, Alaska, and basin temperature is varied, Eq. (10) indicates that there will be a 22% increase in sediment load for every 2 °C warming of the drainage basin. Because Eq. (10) is a steady state predictor, it is not known how long a transition period will be to reach this increase in sediment load. Because Eq. (10) is a function of 20th century basin temperature, and even larger temperatures have occurred during the last 100 years since the Little Ice Age (Syvitski, 2002), change in sediment load due to climate warming would likely occur within decades.

Changes in mean annual runoff may also occur as a result of changes in the regional or continental water balance through hydrological feedbacks with changes in atmospheric circulation (Vörösmarty et al., 2001). Eq. (14) can predict a river's sediment load to the same accuracy as Eq. (10) (see Tables 4 and 6), although some rivers are better predicted by Eq. (10) and others by Eq. (14). Eq. (14) indicates that a 20% increase in discharge, without any intervening basin warming, will result in a 10% increase in sediment transport in the Colville River. When a basin warming of 2 °C is combined with a 20% increase in runoff, then the sediment load of the Colville would increase by 32%.

11. Application of the load model to paleo environments

Over the Holocene period, sea level fluctuations will greatly impact the drainage areas of rivers, although denudation rates are still too slow to impact the relief of these basins. Mulder and Syvitski (1996) examined the impact of sea level recovery since the last ice age on drainage basin area. Although basin area will increase for all non-glacial river basins, most basins show only a limited increase in their drainage area. In the landscape surrounding the large ice sheets, isostatic rebound causes a decrease in their drainage area, although most of these rivers also show limited change in their drainage area. In most cases the increase or decease is within a factor of two. For rivers fronted by a wide continental shelf the small rivers may become tributaries of the larger rivers, or in some cases large rivers will merge to form giant rivers (Mulder and Syvitski, 1996). Eq. (10) will show the largest impact from these large-scale merges.

Polar and even temperate river basins may have seen a 10 °C fluctuation between ice age and modern climate, with concomitant but smaller variations in precipitation. On a tropical river, such as the Fly, Papua New Guinea, the associated change from ice-age temperature would be of a much smaller magnitude. If the temperature changed by 2 °C, the sediment load would increase or decrease by 18% (Fig. 9). If the precipitation on the Fly would have changed by 20%, the sediment load would increase or decrease by 12%. For the Fly, the observed sediment load value (951 kg/s) was most closely predicted from the discharge formula (14) at 883 kg/s, compared to the area formula (10) at 467 kg/s.

While not an exhaustive study, these few examples show how the proposed sediment load model can provide insight into the impact of fluctuations in sea level, temperature and precipitation. Those working on sediment mass balance studies in the offshore (e.g. Nittrouer, 1999) may find the model a useful tool in their paleoclimate investigations. Changes in regional sediment accumulation rates could be used in Eqs. (10) and (14) in the inverse sense, where temperature, discharge, or basin areas are varied to provide a spectrum of possible sediment volumes for comparison to mapped sedimentary deposits.

As an important caveat, Meade (1996) reminds us that global load values (whether observed or predicted) are not exactly the sediment flux to the coastal ocean, but flux estimates of the most seaward gauging stations. These stations are often located well inland, and seaward filters such as deltaic and tidal flats often influence the magnitude of the sediment load reaching the coastal ocean. In the case of the Amazon, 20% (Meade, 1996) to 30% (Nittrouer et al., 1995) of the annually delivered load (1 BT/year) is retained by its delta; the remainder is deposited on the continental shelf and coast. In the case of the Ganges and Brahmaputra Rivers, 32% (Goodbred and Kuehl, 1999) to 55% (Meade, 1996) of their combined annual sediment load (1.1 BT/year) is retained by their delta, with the remainder reaching the shelf and deep sea. In the case of the Yellow River, 82% (Meade, 1996) of the annual load (1.1 BT/year) is retained by its delta; the remainder

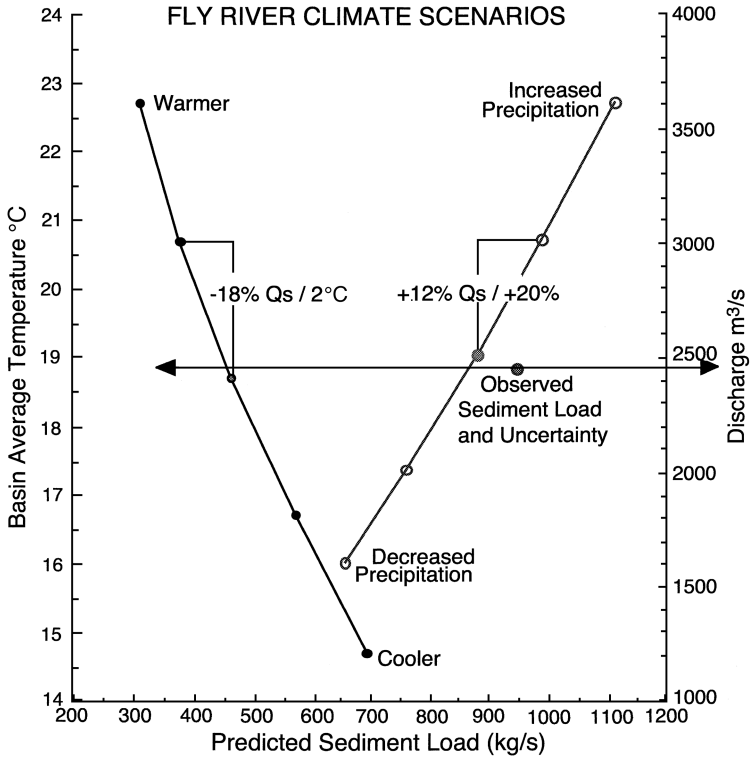

Fig. 9. Example on the effect of climate change on a tropical river, the Fly situated in Papua New Guinea. In this case the discharge formula (14) provides a more accurate prediction of the observed value, as compared to the area formula (10). As temperature increases by 2 °C, the sediment load decreases (non-linearly) by 18%. As the precipitation increases by 20%, and with a concomitant increase in discharge, the sediment load increases by 12%.

deposited on the shelf and coast. Until a method is developed to estimate this filtering effect, Eqs. (10) or (14) provide maximum estimates of sediment available to be spread across shelves and down continental slopes.

12. Summary

We have presented a model for predicting the long-term flux of sediment from river basins to the coastal ocean that requires only a small number of input parameters, namely basin area (or basin discharge), basin relief, basin-averaged temperature and basin location (latitude and longitude). Basin area and relief can be measured with GIS (geographic information system) software, and we provide a formula for estimating mean annual temperature from a knowledge of latitude, longitude and elevation that is locally accurate to within 3 °C. We provide a method for estimating model uncertainty as a function of uncertainty in the input parameters and for ranking the uncertainty that is contributed by each input parameter. The uncertainty in basin temperature makes the largest contribution to uncertainty in the long-term sediment discharge prediction. Application of the model to pre-Quaternary times will result in greater uncertainties in basin area and relief.

Our formula for mean annual temperature incorporates data on lapse rates from a global grid (2.5°) and long-term (>50 year) annual temperatures from 3423 meteorological stations distributed around the world. Algorithms are derived to relate lapse rate with latitude. Once the effect of elevation is incorporated, local temperature can be derived as a function of latitude, but with distinct "arms" for latitudes greater

than 28° north. These two arms are almost entirely due to whether prevailing winds at the station were coming from land or from the sea. A simple rule, based on latitude and longitude, allows for deciding which arm a station would plot on. Further refinement may be possible and is a goal in our effort to reduce uncertainty in our predicted sediment discharges.

When developing predictive formulas for global use, it is important to distinguish between different sources of uncertainty. Given a predictive model formula that depends on several input variables, a well-known theorem makes it possible to estimate how much of the discrepancy between observations and predictions can be attributed to errors in the input variables. The observations on sediment load in our database of 340 river basins have the same magnitude of uncertainties as the model predictions; more certain observations must become available in order to test improvements to the model.

Our sediment discharge model produces predictions within a factor of two for 75% of the rivers in our database, across five orders of magnitude in basin area and discharge. Most of the outliers in the model-data comparison are the result of either sediment trapping in lakes or reservoirs, or from land use practices that result in excessive sediment discharge. Engineering formulas provide an effective way of addressing the issue of sediment retention due to reservoirs. However, there is no global formula for taking into account anthropogenic impacts on soil erosion. Our model can help in identifying problems in the observational data set, whether due to human error, quality of sampling, time span and frequency of sampling, or other extraordinary influences (i.e. unique geology, geography).

Finally, we have provided examples to illustrate how the model can also be applied to global warming studies and the examination of paleo-climate scenarios (warmer/colder; wetter/drier). These examples show the utility of this kind of model, particularly in cases where observational data is unavailable. There are possibly 800 rivers with known sediment load estimates or measurements (J.D. Milliman, personal communication, 2000), but reliable measurements are arguably known for 300 rivers. Our method provides a mechanism for fast and reliable predictions of the sediment loads for the thousands of rivers that have had no sediment load determination.

Acknowledgements

This paper adds to the findings of Nelly Bobrovitskaya, Bob Meade, Michel Meybeck, John Milliman, Yoshi Saito, Charlie Vörösmarty, Des Walling, Mark Morehead and Bob Wasson. The authors have worked closely with these scientists and thank them for their on going support. John Milliman and Steve Kuehl helped the authors sharpen the impact of the paper's thesis. The U.S. Office of Naval Research supported the research behind this paper. This paper forms a contribution to the IGBP Land-Ocean Interaction in the Coastal Zone (LOICZ) program.

References

Ahnert, F., 1970. Functional relationships between denudation, relief, and uplift in large mid-latitude drainage basins. American Journal of Science 268, 243–263.

Andrews, J.T., Syvitski, J.P.M., 1994. Sediment fluxes along high latitude glaciated continental margins: Northeast Canada and Eastern Greenland. In: Hay, W. (Ed.), Global Sedimentary Geofluxes. National Academy of Sciences Press, Washington, pp. 99–115.

Berner, R.A., 1978. Rate control of mineral dissolution under Earth surface conditions. American Journal of Science 278, 1235–1252.

Berner, E.K., Berner, R.A., 1987. The Global Water Cycle: Geochemistry and Environment. Prentice-Hall, Englewood Cliffs, NJ. 397 pp.

Bobrovitskaya, N.N., Skakalsky, B.G., Zubkova, K.M., Dobrotvorskaya, G.I., Petrova, I.V., Tsivjyan, M.V., Chistyakova, N.I., Yanuta, V.G., Callender, E.C., Landa, E.R., Meade, R.H., Councell, T.B., Bruce, R.A., 1997. Hydrologic and hydrochemical data for the Ob-Irtysh and Yenisey River systems of Central Russia, 1954–1988. U.S.G.S. Open File Report 97-232.

Brune, G.M., 1953. Trap efficiency of reservoirs. Transactions American Geophysical Union 34, 407–418.

Douglas, J., 1967. Man, vegetation and the sediment yield of rivers. Nature 215, 925–928.

Edwards, M., 1989. Global Gridded Elevation and Bathymetry (ETOPO5), Digital Raster Data on a 5-Minute Geographic Grid. NOAA National Geophysical Data Center, Boulder, CO.

Fournier, F., 1960. Climat et Erosion. Presses Universitaires de France, (Climate and Erosion) Paris.

Garrels, R.M., Mackenzie, F.T., 1971. Evolution of Sedimentary Rocks. Norton, New York, NY. 397 pp.

Goodbred, S.L., Kuehl, S.A., 1999. Holocene and modern sediment budgets for the Ganges-Brahmaputra River: evidence for high-stand dispersal to flood-plain, shelf, and deep-sea depocenters. Geology 27, 559–562.

Harrison, C.G.A., 1994. Rates of continental erosion and mountain building. Geologische Runschau 83, 431–447.

Harrison, C.G.A., 2000. What factors control mechanical erosion rates? International Journal of Earth Sciences 88, 752–763.

Hay, W.H., 1994. Pleistocene-Holocene fluxes are not the earth's norm. In: Hay, W. (Ed.), Global Sedimentary Geofluxes. National Academy of Sciences Press, Washington, pp. 15–27.

Hay, W.W., Rosol, M.J., Jory, D.E., Sloan II, J.L., 1987. Tectonic control of global patterns and detrital and carbonate sedimentation. In: Doyle, L.J., Roberts, H.H. (Eds.), Carbonate Clastic Transitions: Developments in Sedimentology. Elsevier, Amsterdam, pp. 1–34.

Holeman, J.N., 1980. Erosion rates in the U.S. estimated from the Soil Conservation Services inventory. EOS Transactions of the AGU 61, 954.

Holland, H.D., 1981. River transport to the oceans. In: Emiliani, C. (Ed.), The Sea. The Ocean Lithosphere, vol. 7. John Wiley & Sons, New York, N.Y., pp. 763–800.

Hu, D., Saito, Y., Kempe, S., 2001. Sediment and nutrient transport to the coastal zone. In: Galloway, J.N., Melillo, J.M. (Eds.), Asian Change in the Context of Global Climate Change: Impact of Natural and Anthropogenic Changes in Asia on Global Biogeochemical Cycles. IGBP Publ. Series, vol. 3. Cambridge Univ. Press, Cambridge, UK, pp. 245–270.

Inman, D.L., Jenkins, S.A., 1999. Climate change and the episodicity of sediment flux of small California rivers. Journal of Geology 107, 251–270.

Jansen, J.M., Painter, R.B., 1974. Predicting sediment yield from climate and topography. Journal of Hydrology 21, 371–380.

Kao, S.-J., Liu, K.-K., 2001. Estimating the suspended sediment load by using the historical hydrometric record from the Lanyang-Hsi Watershed. TAO 12, 401–414.

Kao, S.-J., Liu, K.-K., 2002. Exacerbation of erosion induced by human perturbation in a typical Oceania watershed: insight from 45 years of hydrological records from the Lanyang-Hsi River, northeastern Taiwan. Global Biogeochemical Cycles 16, 1–7.

McCave, I.N., 1984. Erosion, transport and deposition of fine-grained marine sediments. In: Stow, D.A.V., Piper, D.J.W. (Eds.), Fine-Grained Sediments: Deep-Water Processes and Facies. Blackwell Scientific Publ., Oxford, pp. 35–69.

Meade, R.H., 1996. River–sediment inputs to major deltas. In: Milliman, J.D., Haq, B.U. (Eds.), Sea-Level Rise and Coastal Subsidence. Kluwer Academic Publishing, Dordrecht, pp. 63–85.

Meybeck, M.M., Ragu, A., 1996. GEMS/Water Contribution to the Global Register of River Inputs. GEMS/Water Programme (UNEP/WHO/UNESCO). World Health Organization, Geneva, Switzerland.

Meybeck, M., Laroche, L., Darr, H.H., Syvitski, J.P.M., 2003. Global variability of total suspended solids and their fluxes in rivers. Global and Planetary Change (in press).

Milliman, J.D., Meade, R.H., 1983. Worldwide delivery of river sediment to the oceans. Journal of Geology 91, 1–21.

Milliman, J.D., Syvitski, J.P.M., 1992. Geomorphic/tectonic control of sediment discharge to the ocean: the importance of small mountainous rivers. Journal of Geology 100, 525–544.

Milliman, J.D., Qin, Y.S., Ren, M.E.Y., 1987. Man's influence on the erosion and transport of sediment by Asian rivers: the yellow River (Huanghe) example. Journal of Geology 95, 751–762.

Milliman, J.D., Rutkowski, C., Meybeck, M., 1995. River Discharge to the Sea: A Global River Index (GLORI). LOICZ Reports and Studies No. 2. (draft version-limited copies available: http://kellia.nioz.nl/loicz/firstpages/products/fp-products.htm).

Mulder, T., Syvitski, J.P.M., 1995. Turbidity currents generated at river mouths during exceptional discharge to the world oceans. Journal of Geology 103, 285–298.

Mulder, T., Syvitski, J.P.M., 1996. Climatic and morphologic relationships of rivers. Implications of sea level fluctuations on river loads. Journal of Geology 104, 509–523.

Nittrouer, C.A., 1999. STRATAFORM: overview of its design and synthesis of its results. Marine Geology 54, 3–12.

Nittrouer, C.A., Kuehl, S.A., Sternberg, R.W., Figueiredo, A.G., Faria, L.E.C., 1995. An introduction to the geological significance of sediment transport and accumulation on the Amazon continental shelf. Marine Geology 125, 177–192.

Pinet, P., Souriau, M., 1988. Continental erosion and large-scale relief. Tectonics 7, 563–582.

Summerfield, M.A., Hulton, N.J., 1994. Natural controls of fluvial denudation rates in major world drainage basins. Journal of Geophysical Research 99, 13871–13883.

Syvitski, J.P.M., 2002. Sediment discharge variability in Arctic rivers: implications for a warmer future. Polar Research 21, 323–330.

Syvitski, J.P.M., 2003. Supply and flux of sediment along hydrological pathways: research for the 21st Century. Global and Planetary Change (in press).

Syvitski, J.P.M., in press, Sediment Fluxes and Rates of Sedimentation. In: G.V. Middleton (Ed.), Encyclopedia of Sediments and Sedimentary Rocks. Kluwer Academic Publishers, Dordrecht, Netherlands.

Syvitski, J.P.M., Andrews, J.T., 1994. Climate Change: numerical modeling of sedimentation and coastal processes, Eastern Canadian Arctic. Arctic and Alpine Research 26, 199–212.

Syvitski, J.P.M., Morehead, M.D., 1999. Estimating river–sediment discharge to the ocean: application to the Eel Margin, northern California. Marine Geology 154, 13–28.

Syvitski, J.P.M., Morehead, M., Nicholson, M., 1998. HydroTrend: a climate-driven hydrologic-transport model for predicting discharge and sediment to lakes or oceans. Computers and Geoscience 24, 51–68.

Syvitski, J.P.M., Morehead, M.D., Bahr, D., Mulder, T., 2000. Estimating fluvial sediment transport: the Rating Parameters. Water Resource Research 36, 2747–2760.

Taylor, J.R., 1982. An Introduction to Error Analysis: The Study of Uncertainties in Physical Measurements. University Science Books, Sausalito, CA.

Trenberth, K.E., 1992. Global analyses from ECMWF and Atlas of 1000 to 10 mb Circulation Statistics. National Center for Atmospheric Research, Boulder, CO. Tech. Rep. NCAR/TN-373 + STR (http://iridl.ldeo.columbia.edu/SOURCES/.ECMWF/.GGA/.psfc/).

Verstraeten, G., Poesen, J., 2000. Estimating trap efficiency of small reservoirs and ponds: methods and implications for the assessment of sediment yield. Progress in Physical Geography 24, 219–251.

Vörösmarty, C.J., Meybeck, M., Fekete, B., Sharma, K., 1997. The potential impact of neo-Castorization on sediment transport by

the global network of rivers. In: Walling, D., Probst, J.-L. (Eds.), Human Impact on Erosion and Sedimentation. IAHS Press, Wallingford, UK, pp. 261–272.

Vörösmarty, C.J., Fekete, B.M., Meybeck, M., Lammers, R., 2000a. Geomorphometric attributes of the global system of rivers at 30-minute spatial resolution (STN-30). Journal of Hydrology 237, 17–39.

Vörösmarty, C.J., Fekete, B.M., Meybeck, M., Lammers, R., 2000b. Global system of rivers: Its role in organizing continental land mass and defining land-to-ocean linkages. Global Biogeochemical Cycles 14, 599–621.

Vörösmarty, C.J., Hinzman, L.D., Peterson, B.J., Bromwich, D.H., Hamilton, L.C., Morrison, J., Romanovsky, V.E., Sturm, M., Webb, R.S., 2001. The hydrological cycle and its role in Arctic and global environmental change: A rationale and strategy for synthesis study, Arctic Research Consortium of the U.S., Fairbanks.

Vorosmarty, C., Meybeck, M., Fekete, B., Sharma, K., Green, P., Syvitski, J.P.M., 2003. Anthropogenic sediment retention: major global-scale impact from the population of registered impoundments. Global and Planetary Change (in press).

Wallace, J.M., Hobbs, P.V., 1977. Atmospheric Science: And Introductory Survey. Academic Press, New York.

Walling, D.E., 1987. Rainfall, runoff, and erosion of the land: a global view. In: Gregory, K.J. (Ed.), Energetics of Physical Environment. Wiley, London, UK, pp. 89–117.

Wang, Y., Ren, M.-E., Syvitski, J.P.M., 1998. Sediment transport and terrigenous fluxes. In: Brink, K.H., Robinson, A.R. (Eds.), The Sea: Vol. 10—The Global Coastal Ocean: Processes and Methods. Wiley, New York, pp. 253–292.

Ward, P.R.B., 1980. Sediment transport and a reservoir siltation formula for Zimbabwe–Rhodesia. Die Siviele Ingenier in Suid-Afrika, 9–15 (Januarie).

Wasson, R.J., 1996. Land use and climate impacts on fluvial systems during the period of agriculture. PAGES Workshop Report, Series 96-2.

Wilson, L., 1973. Variations in mean annual sediment yield as a function of mean annual precipitation. American Journal of Science 273, 335–349.